Steady-State Gating of Batrachotoxin-modified Sodium Channels

Variability and Electrolyte-dependent Modulation

L. D. CHABALA, B. W. URBAN, L. B. WEISS, W. N. GREEN, and O. S. ANDERSEN

From the Department of Physiology and Biophysics and Department of Anesthesiology, Cornell University Medical College, New York 10021; and Department of Medicine, Jefferson Medical College, Philadelphia, Pennsylvania 19107

ABSTRACT   The steady-state gating of individual batrachotoxin-modified sodium channels in neutral phospholipid bilayers exhibits spontaneous, reversible changes in channel activation, such that the midpoint potential (V_a) for the gating curves may change, by 30 mV or more, with or without a change in the apparent gating valence (z_a). Consequently, estimates for V_a and, in particular, z_a from ensemble-averaged gating curves differ from the average values for V_a and z_a from single-channel gating curves. In addition to these spontaneous variations, the average V_a shifts systematically as a function of [NaCl] (being -109, -88, and -75 mV at 0.1, 0.5, and 1.0 M NaCl), with no systematic variation in the average z_a (~ 3.7). The [NaCl]-dependent shifts in V_a were interpreted in terms of screening of fixed charges near the channels' gating machinery. Estimates for the extracellular and intracellular apparent charge densities ($\sigma_e = -0.7$ and $\sigma_i = -0.08$ e/nm^2) were obtained from experiments in symmetrical and asymmetrical NaCl solutions using the Gouy-Chapman theory. In 0.1 M NaCl the extracellular and intracellular surface potentials are estimated to be -94 and -17 mV, respectively. The intrinsic midpoint potential, corrected for the surface potentials, is thus about -30 mV, and the standard free energy of activation is approximately -12 kJ/mol. In symmetrical 0.1 M NaCl, addition of 0.005 M Ba^{2+} to the extracellular solution produced a 17-mV depolarizing shift in V_a and a slight reduction in z_a. The shift is consistent with predictions using the Gouy-Chapman theory and the above estimate for σ_e. Subsequent addition of 0.005 M Ba^{2+} to the intracellular solution produced a ~ 5-mV hyperpolarizing shift in the ensemble-averaged gating curve and reduced z_a by ~ 1. This Ba^{2+}-induced shift is threefold larger than predicted, which together with the reduction in z_a implies that Ba^{2+} may bind at the intracellular channel surface.

Dr. Chabala's present address is Department of Medicine, Jefferson Medical College, Philadelphia, PA 19107. Dr. Weiss's present address is Anesthesiology Scientific Solutions, 79 Riverton Drive, San Francisco, CA 94132. Dr. Green's present address is Department of Cellular and Molecular Physiology, Yale University School of Medicine, New Haven, CT 06510.

INTRODUCTION

The voltage activation, or gating, of sodium channels in excitable cell membranes is modulated by changes in the extracellular (Frankenhaeuser and Hodgkin, 1957; Hille, 1968; Brismar, 1973; Begenisich, 1975; Hille et al., 1975; Århem, 1980) or intracellular (Chandler et al., 1965; Begenisich and Lynch, 1973) electrolyte composition. These electrolyte-dependent changes in channel gating appear to result predominantly from changes in the extracellular and intracellular surface potentials. These changes are brought about by specific ion adsorption to the channel or the surrounding host bilayer (Frankenhaeuser and Hodgkin, 1957; Begenisich and Lynch, 1973; Grissmer, 1984), by electrolyte screening of fixed surface charges (Chandler et al., 1965), or by a combination of these mechanisms (Begenisich, 1975; Hille et al., 1975; Århem, 1980). Apart from this electrolyte-dependent modulation, however, voltage-dependent gating is usually considered to be an invariant characteristic of sodium channel activation, befitting its physiological importance in the generation of propagated action potentials.

We wished to examine the electrolyte-dependent modulation of the steady-state gating of bilayer-incorporated batrachotoxin (BTX)-modified sodium channels in order to ascertain the importance of channel-associated charges and to determine whether there is an asymmetrical surface charge density near the voltage-sensing region. When pursuing these questions, however, we observed a large variability in gating behavior (Green et al., 1984; Weiss et al., 1984), such that spontaneous changes in single-channel gating curves could be larger than experimentally imposed electrolyte-dependent changes. In a single channel, successive gating curves could differ much more than could be accounted for by the statistical uncertainty of the measurements (intrachannel variability); when comparing results obtained with different channels, the gating curves could again differ much more than expected (interchannel variability).

We demonstrate the intrinsic variability in the steady-state gating of single BTX-modified sodium channels from canine forebrain and examine the electrolyte-dependent modulation of the steady-state gating based on either the average behavior of individual gating curves or ensemble-averaged gating curves generated from the experiments on single channels. The experiments were done on channels incorporated into net neutral phospholipid bilayers, such that effects that can be ascribed to surface charges result from charges on the channel itself. To minimize complications resulting from specific cation adsorption (Begenisich, 1975; Hille et al., 1975; Århem, 1980; Cukierman et al., 1988), the extracellular and intracellular charge densities were estimated based on experiments at different monovalent salt (NaCl) concentrations or the addition of Ba^{2+} (asymmetrically or symmetrically) to channels bathed in 0.1 M NaCl. For either set of experiments, the results indicate that there is a net negative charge density at both channel surfaces. Based on experiments in which only the [NaCl] was changed, the extracellular apparent charge density (-0.7 $e \cdot nm^{-2}$) is estimated to be ~10-fold larger in magnitude than the intracellular apparent charge density (-0.08 $e \cdot nm^{-2}$). Consequently, at 0.1 M NaCl the intrinsic (surface potential–corrected) activation midpoint potential is ~75 mV more positive than the measured value (-110 mV), which must be taken into account when estimating the standard free energy for channel activation.

Preliminary reports of this work have been presented (Green et al., 1984; Weiss et al., 1984; Chabala et al., 1989).

MATERIALS AND METHODS

Materials

1-Palmitoyl-2-oleoyl-phosphatidylethanolamine (PE) and -phosphatidylcholine (PC) were from Avanti Polar Lipids (Pelham, AL). n-Decane was from Wiley Organics (Columbus, OH).

Inorganic salts and HEPES were reagent grade. The NaCl was roasted at 500–600°C for 24 h to remove organic impurities. The water was deionized Milli-Q water (Millipore Corp., Bedford, MA). The NaCl solutions were buffered to pH 7.4 using 10 mM phosphate or HEPES.

Canine forebrain synaptosomal membrane fractions were prepared as described by Cohen et al. (1977). BTX was a generous gift from Dr. John Daly (National Institutes of Health, Bethesda, MD).

Membrane Formation

Planar bilayers were formed at room temperature (21–26°C) from a 4:1 solution of PE and PC in n-decane (5% wt/vol) across a 300-μm-diam hole in a 125-μm-thick Teflon partition as described previously (Green et al., 1987).

Channel Incorporation

Sodium channels were modified using BTX, which permits steady-state gating to be studied (Krueger et al., 1983). BTX was added to one side of the bilayer to a nominal concentration between ~0.04 and 0.8 μM. In the experiments at low aqueous BTX concentrations, BTX was also added (to a nominal concentration of ~1 μM) to the vial containing the synaptosomal preparation.

Sodium channel incorporation was achieved as described in Green et al. (1987), with the following modification: in some experiments a membrane-forming bubble was blown across the hole in the Teflon partition; after the membrane had thinned, the pipette was dipped into the vial containing the synaptosomal membranes and a new membrane was formed. This yielded a high success rate for channel incorporation, usually after a waiting time of several minutes. If there was no incorporation after ~10 min, the procedure was repeated until incorporation occurred or the membranes failed to thin properly.

Once a channel had incorporated, it was tested to determine if it was a BTX-modified sodium channel using the criteria outlined in Green et al. (1987).

Electrical Measurements

Single-channel currents were recorded using a two-electrode voltage clamp, either home-built or an Axopatch 1B (Axon Instruments, Inc., Foster City, CA), with contact to the aqueous solutions through Ag/AgCl electrodes: the *cis* electrode was in direct contact to that solution; the *trans* electrode was a Ag/AgCl pellet in a microelectrode holder with contact to the solution through an L-shaped glass pipette (see Green et al., 1987, for further details).

All results are reported using the electrophysiological sign convention: the aqueous phase facing the tetrodotoxin binding site on the channel is the reference, irrespective of the channel's orientation in the membrane. This reference solution is the "extracellular" solution; the other is the "intracellular" solution.

Before each experiment, the electrodes were balanced and care was taken to ensure minimal drift. In experiments with asymmetrical and symmetrical $BaCl_2$ addition, the membrane potential was corrected for the half-cell potential at the *cis* electrode (V_{hc} = 2.4 mV) associated

with $BaCl_2$ addition to the *cis* solution and the liquid-junction potential at the pipette-solution junction in the *trans* chamber ($V_{lj} = -1.2$ mV) associated $BaCl_2$ addition to the *trans* solution: $V = V_{ap} - (V_{hc} + V_{lj})$, where V_{ap} is the nominally applied potential. V_{lj} was estimated by the Henderson equation (Henderson, 1907), using limiting equivalent conductivities (Robinson and Stokes, 1965, Appendix 6.2).

Experimental Protocols

Channel activation was quantified as the fractional channel open time (f_o), which was evaluated by using two different protocols. In either case, f_o was estimated from measurements of the time-averaged membrane current (I_m) after correcting for the background leak conductance (see below).

The initial experiments (protocol I) were done using a low-pass integrator (Andersen and Muller, 1982) to obtain an analogue representation of the time-averaged single-channel current. The membrane potential was varied manually in 5–100-mV (usually 10-mV) steps, with 10–60-s sojourns at each level. The output from the current-to-voltage converter was amplified and displayed on two channels of a stripchart recorder. The output on one of the channels was filtered at 10–100 Hz and used to visualize individual single-channel open↔close transitions. The output on the other channel was filtered at 0.1–1 Hz to measure I_m, which was estimated from 10-s segments chosen to eliminate gating state changes (e.g., Fig. 2).

The subsequent experiments (protocol II) were done using a fixed protocol under computer control: first, the membrane potential (V) was held at +60 mV for 2 min to establish a well-defined initial state and to minimize slow capacitative transients in the solvent-containing bilayer; V was then stepped in 10-mV increments (of 5 s duration) from +60 mV to between −110 and −130 mV (hyperpolarizing sequence), and back to +60 mV (depolarizing sequence). Most of the fast capacitative transient was removed by subtracting the current trace at 0 mV from all other current traces (any remaining transient was "removed" by ignoring the first 0.6 s of each step in the subsequent analysis), and the time-averaged "difference current" was calculated for last 4.4 s of each step, whether or not a gating state change occurred during the 5 s. (Divalent cations may permeate through BTX-modified sodium channels [Khodorov and Revenko, 1979]. At 0 mV, in the presence of asymmetrical Ba^{2+}, there may thus be a finite current through the open channel, which would offset the difference traces. But any offset will be the same at all potentials and will not affect our estimates of V_a or z_a.) For each gating run, two steady-state gating curves were thus constructed: one based on the hyperpolarizing sequence, and (if the membrane had not broken) one based on the depolarizing sequence.

To minimize bias resulting from membrane breakage at large negative potentials, the following precautions were taken: electrolyte and lipid solutions were fresh, and only a very small amount of membrane vesicles was added. In addition, in experiments using protocol II, the duration of the potential was limited to 5 s (which in itself decreases the probability of membrane breakdown), and the potential span was set in advance (i.e., without knowledge of the channel's gating pattern). Channels were lost because of membrane breakage, which results in a smaller number of depolarizing sequences (Tables I and IV); but that probably did not introduce a systematic bias because the average V_a was similar for the hyperpolarizing and depolarizing sequences in 0.1 M NaCl, where the problem should be most pronounced (cf. Table I).

Data Analysis

To estimate f_o, $I_m(V)$ was corrected for the bilayer background conductance (G_b), which was assumed to be voltage independent and was estimated from long spontaneous channel closures, usually at the extreme hyperpolarizing potentials where the channels were mostly closed. $f_o(V)$ was then calculated as:

$$f_o(V) = [I_m(V) - G_b \cdot V]/[n \cdot g(V) \cdot V] \tag{1}$$

where n is the number of channels in the membrane and $g(V)$ is the single-channel conductance. It was not possible to determine $g(V)$ for each channel from discrete current transitions throughout the entire gating region. $g(V)$ was therefore determined by constructing average single-channel current–voltage (i-V) relations by scanning the individual current records (obtained using protocol II) at each potential and identifying transitions of sufficient duration that the closed and open current levels could be determined.

The results were analyzed using a two-state model, in which channel activation/deactivation is assumed to occur as voltage-dependent transitions between two channel states: a low-conductance, or closed, state and a high-conductance, or open, state (Mueller and Rudin, 1963). In this approximation, the steady-state f_o-V relation is given by (e.g., Ehrenstein et al., 1970):

$$f_o = f_{o,max}/\{1 + \exp[-z_a \cdot e \cdot (V - v_a)/kT]\}$$ (2)

where $f_{o,max}$ is the maximal fractional open time, z_a is the apparent gating valence (the apparent number of elementary charges that move, from inside to outside, during channel opening, irrespective of the molecular mechanism underlying channel activation [e.g., Armstrong, 1981]), e is the elementary charge, V_a is the midpoint potential (the potential at which $f_o = f_{o,max}/2$), k is Boltzmann's constant, and T is the temperature in degrees Kelvin. In the two-state approximation, $f_{o,max}$ should be 1.0. In practice, $f_{o,max}$ is <1.0 because voltage-independent channel closures occur at all membrane potentials (Moczydlowski et al., 1984; Green et al., 1987).

Combining Eqs. 1 and 2, one obtains the following expression:

$$I_m(V) - G_b \cdot V = n \cdot g(V) \cdot f_{o,max} \cdot V/\{1 + \exp[-z_a \cdot e \cdot (V - V_a)/kT]\}$$ (3)

which was fitted to the results using a nonlinear least-squares fit implementing the Marquardt algorithm (e.g., Bevington, 1969). The advantage of using Eq. 3 rather than Eq. 2 is that the chi-square minimization routine now emphasizes results near V_a, where the current magnitude is largest. One thus determines three independent parameters: $g \cdot f_{o,max}$, z_a, and V_a.

Two different analysis procedures were used. First, each individual (hyperpolarizing or depolarizing) gating sequence was analyzed to obtain information about the intra- and interchannel gating variation. In this analysis, data points that clearly fell far from a monotonic activation/deactivation pattern (cf. open symbols in Figs. 3, 6, and 7) were eliminated from the fits. Second (when using protocol II), for each voltage the results from all sequences (hyperpolarizing or depolarizing) were averaged together, including the points that were eliminated from the individual fits, to obtain the ensemble-averaged gating curves, which were analyzed as described above. For either type of analysis, the hyperpolarizing and depolarizing sequences were analyzed separately to test for stationarity. Data points at $V > 0$ mV were not included in the analysis, because BTX-modified sodium channels often exhibit a "flickery" behavior at these potentials (cf. Green et al., 1987).

Each fitted curve was plotted (as I_m/V [$=G_m$] vs. V, f_o vs. V, and $\log\{f_o/[f_{o,max} - f_o]\}$ vs. V) to verify agreement with the results. In addition, V_a for each gating curve was determined by visual inspection of the current traces and estimation of the potential at which that channel spent half its time in the open state. These subjective estimates never differed by more than a few millivolts from the curve-fit estimates for V_a.

RESULTS

Gating Variability in BTX-modified Sodium Channels

Fig. 1 shows the gating behavior of a bilayer-incorporated BTX-modified sodium channel in symmetrical 0.1 M NaCl using protocol II (see also Moczydlowski et al.,
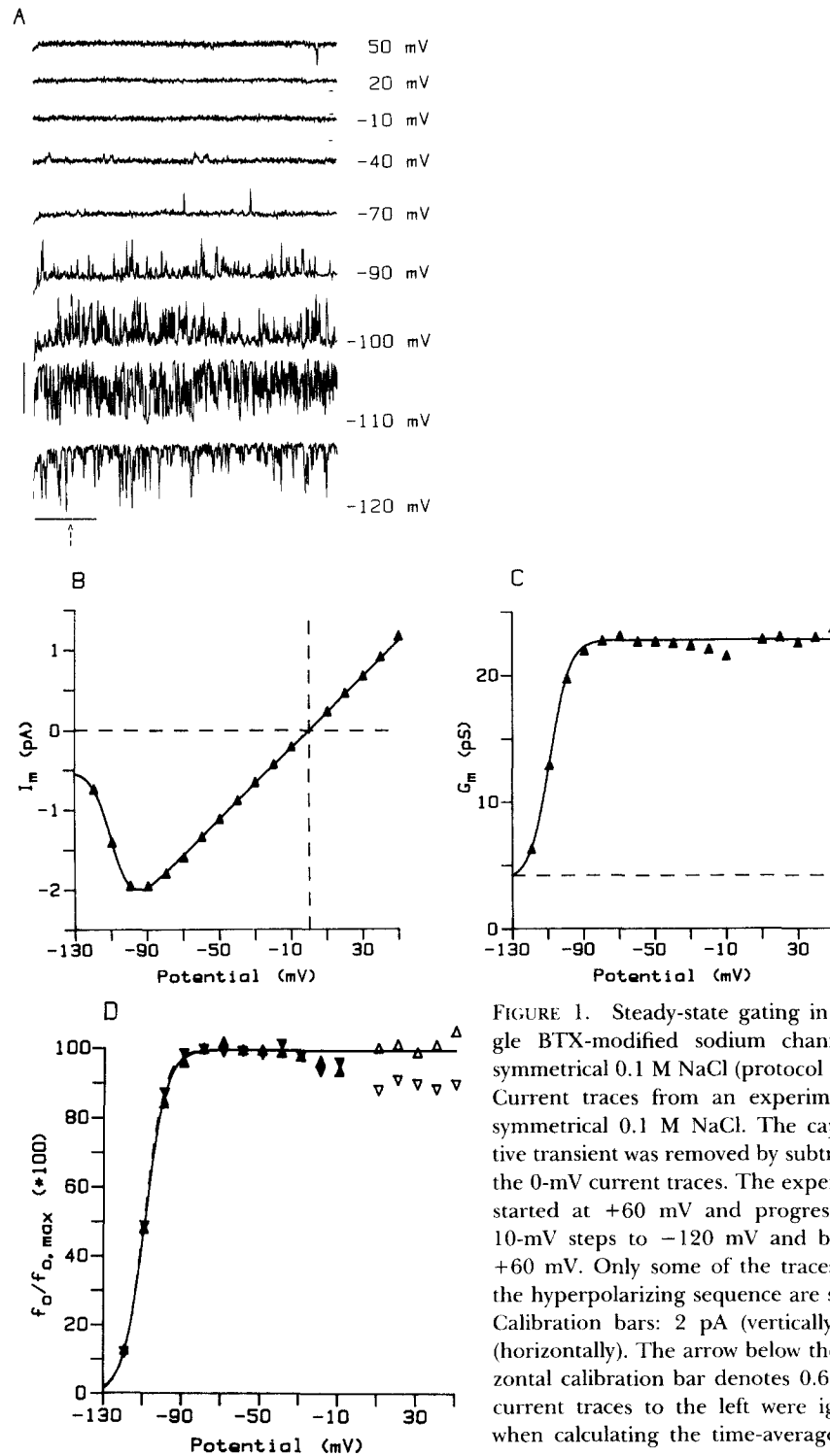
FIGURE 1. Steady-state gating in a single BTX-modified sodium channel in symmetrical 0.1 M NaCl (protocol II). (*A*) Current traces from an experiment in symmetrical 0.1 M NaCl. The capacitative transient was removed by subtracting the 0-mV current traces. The experiment started at +60 mV and progressed in 10-mV steps to −120 mV and back to +60 mV. Only some of the traces from the hyperpolarizing sequence are shown. Calibration bars: 2 pA (vertically); 1 s (horizontally). The arrow below the horizontal calibration bar denotes 0.6 s (the current traces to the left were ignored when calculating the time-averaged dif-
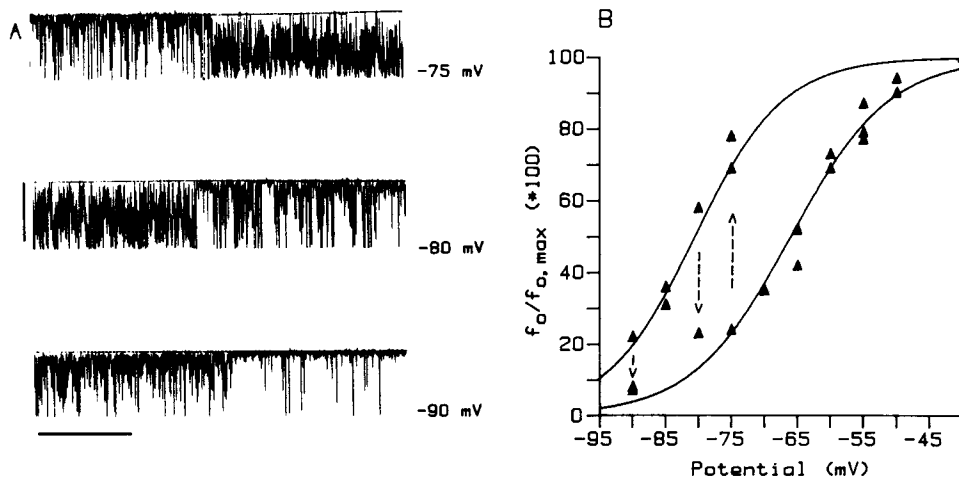
FIGURE 2. Spontaneous gating state changes in a single BTX-modified sodium channel in symmetrical 1.0 M NaCl (protocol I). (*A*) Single-channel current traces depicting discrete changes in channel activity. Channels openings are downward. (*Top*) −75 mV, at the arrow I_m increases from 0.97 to 1.82 pA (f_o increases from 0.24 to 0.69). (*Middle*) −80 mV, at the arrow I_m decreases from 1.73 to 1.04 pA (f_o decreases from 0.58 to 0.23). (*Bottom*) −90 mV, at the arrow I_m decreases from 1.16 to 0.83 pA (f_o decreases from 0.22 to 0.07). The straight lines through the upper envelope of each trace denote the background current through the bilayer ($G_b \approx 7.2$ pS). Calibration bars: 2 pA (vertically), 5 s (horizontally). (*B*) Fractional open time as a function of V; the gating transitions in A are denoted by arrows. Results from a single hyperpolarizing sequence plotted as $f_o/f_{o,max}$ vs. V. The variations in gating behavior are seen as transitions between two approximately parallel activation curves (with $V_a = -82$ or -66 mV, respectively, and $z_a \approx 3.5$). Exp. 120883.

1984; Hartshorne et al., 1985; French et al., 1986; Recio-Pinto et al., 1987; Cukierman et al., 1988). Between +50 and −70 mV (using the electrophysiological sign convention; see Methods) the channel was open most of the time; at −90 mV channel closing transitions increased in frequency; at −110 mV the channel was open ~50% of the time; and at −120 mV the channel was mostly closed (Fig. 1 *A*). The single-channel current (*i*) is a linear function of voltage (*V*), but the time-averaged

ference currents). The horizontal lines toward the right of the 20-, −10-, and −40-mV traces denote the closed state current levels. (*B*) Time-averaged membrane current as a function of *V*. Results from the hyperpolarizing sequence. The curve was calculated using the following parameters: $G_b = 3.9$ pS, $g \cdot f_{o,max} = 18.6$ pS ($g = 19.4$ pS, $f_{o,max} = 0.96$), $V_a = -108.8$ mV, and $z_a = 4.65$. (*C*) Time-averaged membrane conductance as a function of *V*. Results from the hyperpolarizing sequence. The curve was calculated using the parameters in *B*. The interrupted line denotes the background conductance. (*D*) Fractional open time as a function of *V*. *Triangles*, results from hyperpolarizing sequence; *inverted triangles*, results from depolarizing sequence. Only the solid points were used for the curve fit. The continuous curve (for the hyperpolarizing sequence) was calculated using Eq. 2 and the parameters in *B*; the interrupted curve (for the depolarizing sequence) was calculated using Eq. 2: $V_a = -109$ mV and $z_a = 5.1$. Exp. L01.
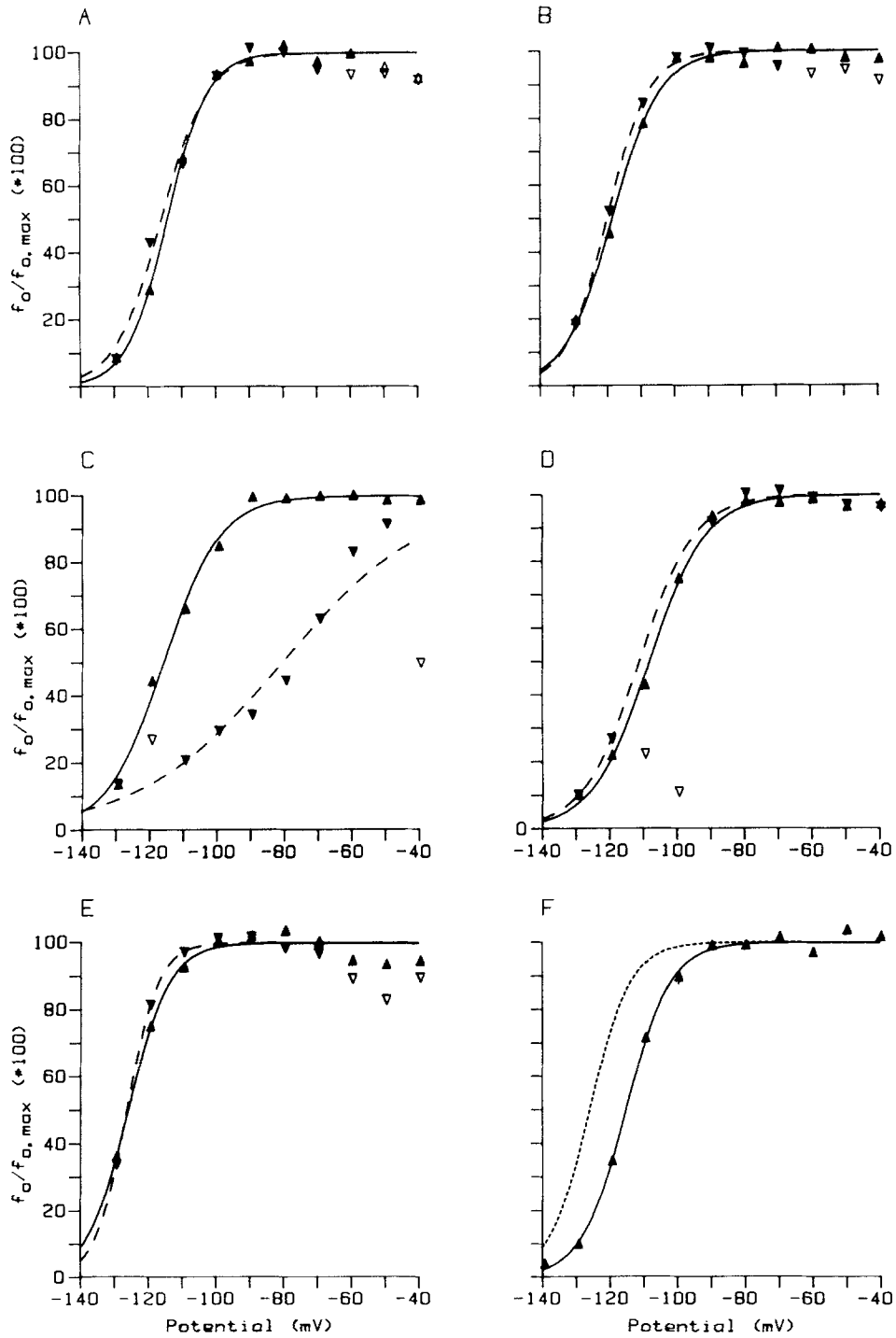
FIGURE 3.

membrane current (I_m) is a nonmonotonic function of V (Fig. 1 B): I_m goes through a minimum, at -90 to -100 mV, and then increases (display a negative slope conductance) until only the background (leak) current remains at very negative voltages. Corresponding to the region of negative slope conductance, the membrane conductance (G_m) varies as a steep, sigmoidal function of V (Fig. 1 C). The time-averaged fractional open time (f_o) was calculated after correcting for the leak conductance (see Methods) and was, again, a steep sigmoidal function of V (Fig. 1 D).

In the experiment in Fig. 1, the gating was regular and stable: the points from the hyperpolarizing and the depolarizing sequences were almost superimposable, and V_a was -109 mV for either set of results. For a given experimental condition, however, V_a would vary by 30 mV or more (see Table I). This variation in V_a results from an intra- as well as interchannel variability in the gating pattern (Figs. 2 and 3).

Fig. 2 illustrates results obtained in 1.0 M NaCl using protocol I. In the current traces (Fig. 2 A) it is apparent that a channel, at a constant V, can undergo abrupt, spontaneous changes in activation (changes in f_o). Corresponding to these changes in f_o, there were discrete, reversible changes in the steady-state gating curve (Fig. 2 B). The individual points tend to fall on parallel lines, shifted ~ 16 mV along the voltage axis. We emphasize that this variability does not result from the statistical uncertainty in estimating I_m (and thus f_o). Rather, it results because a single channel can exist in several different gating states, with slow transitions among the different states that are outside our experimental control.

Fig. 3 depicts results obtained in 0.1 M NaCl using protocol II. The six panels illustrate results from two consecutive gating runs (both hyperpolarizing and depolarizing sequences) in three different experiments with only a single channel in the membrane. These experiments were chosen to illustrate the different gating behaviors that can be observed using a fixed protocol. In the top panels (Fig. 3, A and B), the hyperpolarizing and depolarizing sequences are almost superimposable, and the results of two successive gating runs are comparable. In the next two panels (Fig. 3, C and D), in the first run the depolarizing sequence is shifted in the depolarizing direction and z_a is reduced more than twofold relative to the hyperpolarizing sequence (Fig. 3 C), while the second run demonstrates the nonmonotonic behavior

---

Figure 3. (*opposite*) Gating variability in four BTX-modified single sodium channels in symmetrical 0.1 M NaCl (protocol II). The results are plotted as normalized gating curves ($f_o/f_{o,\mathrm{max}}$) vs. V. For each channel, the two side-by-side panels depict the results of successive gating runs. Triangles denote results from hyperpolarizing sequences and inverted triangles denote results from depolarizing sequences. Closed symbols denote points that were included in the curve fits, and open symbols are points that were omitted. Solid curves denote fits to the hyperpolarizing sequences, and interrupted curves denote fits to the depolarizing sequences. (A and B) Exp. L16. (A) $V_a = -114$ mV, $z_a = 4.3$ (hyperpolarizing); $V_a = -116$ mV, $z_a = 3.7$ (depolarizing). (B) $V_a = -119$ mV, $z_a = 3.6$ (hyperpolarizing); $V_a = -120$ mV; $z_a = 4.1$ (depolarizing). (C and D) Exp. L49. (C) $V_a = -116$ mV, $z_a = 3.0$ (hyperpolarizing); $V_a = -81$ mV, $z_a = 1.2$ (depolarizing). (D) $V_a = -108$ mV, $z_a = 3.0$ (hyperpolarizing); $V_a = -111$ mV, $z_a = 3.1$ (depolarizing). (E and F) Exp. L08. (E) $V_a = -126$ mV, $z_a = 4.2$ (hyperpolarizing); $V_a = -126$ mV, $z_a = 5.5$ (depolarizing). (F) $V_a = 115$ mV, $z_a = 3.9$ (hyperpolarizing); a second channel incorporated early in the depolarizing sequence, which is not illustrated; the stippled line denotes the fit to the hyperpolarizing sequence in E.

that can appear in an otherwise superimposable run (Fig. 3 D). In the bottom panels (Fig. 3, E and F), the first hyperpolarizing and depolarizing sequences are superimposable (Fig. 3 E); in the second run, the hyperpolarizing sequence is shifted ~11 mV in the depolarizing direction, as compared with the first run, with little change in z_a (Fig. 3 F).

In a given experiment there may be many spontaneous changes in f_o, or there may be none (see also Moczydlowski et al., 1984; French et al., 1986; Recio-Pinto et al., 1987). The associated gating variability does not reflect a general channel deterioration (cf. Fig. 3), and since spontaneous changes in f_o were observed with either protocol and with all electrolyte solutions we have used, the existence of different gating behaviors cannot be ascribed to a particular experimental protocol.

TABLE I

Sodium Channel Gating in 0.1 M NaCl

	Hyperpolarizing	Depolarizing	Combined	Range
V_a				
(mV)	-113 ± 8 (50)	-111 ± 13 (39)	-112 ± 11 (89)	$-77/-129$
z_a	3.7 ± 0.9	3.6 ± 1.4	3.7 ± 1.2	$1.2/6.5$
$g \cdot f_{0,max}$				
(pS)	19.3 ± 2.0	19.3 ± 2.1	19.3 ± 2.0	$13.5/23.5$
G_b				
(pS)	5.8 ± 1.7	5.7 ± 1.9	5.7 ± 1.9	$3.2/11.5$
$V_a{}^*$				
(mV)	-112 ± 8 (41)	-110 ± 15 (31)	-111 ± 11 (72)	$-77/-129$
$z_a{}^*$	3.7 ± 1.0	3.8 ± 1.4	3.7 ± 1.2	$1.2/6.5$
$g \cdot f_{0,max}{}^*$				
(pS)	19.4 ± 2.1	19.4 ± 2.2	19.4 ± 2.1	$13.5/23.5$
$g^\ddagger$			20.8 ± 0.5	
$f_{0,max}{}^\S$			0.96	

Results obtained using protocol II. Mean ± SD (number), obtained by averaging data from the individual gating sequences. Results are based on 36 different membranes with one to six channels (72 single-channel gating sequences). V_a, z_a, and $g \cdot f_{0,max}$, denote estimates from the curve fits; G_b denotes the measured background conductance. *Estimates based on the 72 single-channel gating sequences.

‡The average small-signal conductance determined from the aggregate i-V relations (Fig. 5).

§$f_{0,max}$, determined as $g \cdot f_{0,max}/g$.

Average Gating Behavior

The results of fitting all the individual gating runs in symmetrical 0.1 M NaCl using protocol II is summarized in Table I. The results are summarized as V_a, z_a, and $g \cdot f_{o,max}$ for the hyperpolarizing and depolarizing sequences separately and combined (as well as the average small-signal conductance, g, and $f_{o,max}$). There was, as would be expected, a large variability in the parameter estimates, with the largest variability among the depolarizing sequences. A similar difference in variability was found for the subset of 31 single-channel gating runs with paired hyperpolarizing and depolar-

izing sequences. Within this subset, the paired difference in V_a $(V_{a,dep} - V_{a,hyp})$ was $+2.5 \pm 12.7$ mV (mean $\pm$ SD, $n = 31$), which is not significantly different from zero (the differences were not normally distributed, however, as 23 of the 31 gating runs had differences <6 mV). Nevertheless, there may be small differences between the hyperpolarizing and depolarizing sequences if the capacitative current transients are not fully corrected for by subtracting the 0-mV traces.

To overcome the limitations imposed by the gating variability, and the subjectivity inherent in deciding whether to include or exclude an "outlier," we therefore constructed an ensemble-averaged gating curve (based on all the individual gating curves obtained in 0.1 M NaCl using protocol II), where the f_o-V relation was constructed by averaging all the results obtained at a given membrane potential (Fig. 4). When these results were analyzed, by fitting Eq. 3 to the ensemble-averaged I_m-V relation, the estimate for V_a (-114 mV) did not differ significantly from the mean value obtained by averaging V_a for the fits to individual experiments (-112 ± 1 mV,
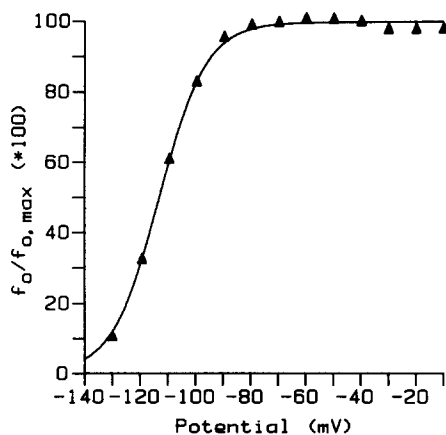

FIGURE 4. Ensemble-averaged gating curves in 0.1 M NaCl. The results from all 89 gating sequences (both hyperpolarizing and depolarizing) obtained using protocol II were averaged and plotted as normalized gating curves ($f_o/f_{o,max}$) vs. V. $V_a = -114$ mV, $z_a = 2.8$.

mean $\pm$ SEM). But the estimate for z_a (2.8) was less than the estimate obtained from averaging the individual fits (3.7). That result is expected because z_a reflects the steepness of the gating curves, and any dispersity in gating behavior would "spread out" the ensemble-averaged gating curve and thus decrease the apparent z_a (with minimal effect on V_a).

Effects of Changing the Monovalent Cation Concentration

In addition to the spontaneous variations in gating behavior described above, V_a varied systematically as a function of the extracellular and intracellular electrolyte composition. In the absence of divalent cations, symmetrical increases in [NaCl], from 0.1 to 1.0 M, produced a 34-mV depolarizing shift in V_a with little change in z_a (Table II). These experiments were done using protocol I (i.e., with unsystematic voltage steps), but the mean value and range of both V_a and z_a (at 0.1 M NaCl) are nevertheless indistinguishable from those obtained with protocol II.

When only the intracellular [NaCl] was changed, from 0.1 to 0.02 M at a constant

TABLE II

Effect of [NaCl] on Sodium Channel Gating

[NaCl]*	V_a	Range	z_a	N_m	N_c
M	mV	mV			
0.1/0.1	-109 ± 10	$-84/-122$	3.8 ± 0.9	14	35
0.5/0.5	-89 ± 11	$-69/-95$	3.8 ± 0.5	5	15
1.0/1.0	-75 ± 8	$-61/-87$	3.4 ± 1.3	5	8
0.1/0.02	-90 ± 11	$-65/-99$		4	6

Results obtained using protocol I. All points for a given membrane was used when fitting Eq. 3 to the results. Means ± SD. N_m and N_c denotes the number of membranes and channels, respectively. The number of channels per membrane varied between one and nine. Statistics based on N_m. *[NaCl]$_e$/[NaCl]$_i$.

extracellular [NaCl] of 0.1 M, the gating curve was shifted ~19 mV in the depolarizing direction (Table II). In these experiments V_a was determined directly as the potential where f_o was ~0.5 and estimates for z_a were not obtained.

Na$^+$ and Cl$^-$ are not expected to bind strongly to net neutral phospholipid bilayers (Gottlieb, 1974) or proteins (Steinhardt and Beychok, 1964). Therefore, the depolarizing shift in V_a as a function of symmetrical increases in [NaCl] most likely results from the screening of fixed charges at one or both channel surfaces (e.g., Gilbert and Ehrenstein, 1984). Qualitatively, a depolarizing shift in V_a as a function of a symmetrical increase in ionic strength would occur when the extracellular surface charge density is more negative (or less positive) than the intracellular surface charge density. A hyperpolarizing shift in V_a as a function of an increased intracellular ionic strength would occur if there is a net negative intracellular surface charge density.

Effects of Changing Divalent Cation Concentration

If the [NaCl]-dependent shifts in V_a indeed result from surface potential changes due to the screening of fixed surface charges, similar shifts should be induced by divalent cations (McLaughlin et al., 1971; Hille et al., 1975). To minimize complications due to "specific" ion adsorption to the channel or bilayer (Begenisich, 1975; Hille et al., 1975; Århem, 1980; Cukierman et al., 1988), this was tested in experiments using Ba^{2+} as the divalent cation. The experiments were done using protocol II.
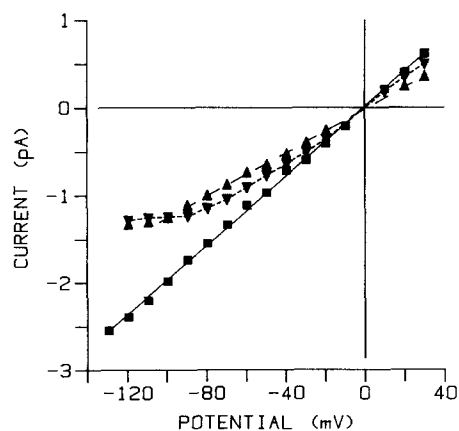

FIGURE 5. *i-V* relations in symmetrical 0.1 M NaCl (*squares* and *solid line*), and after addition of BaCl$_2$ to only the extracellular solution (*inverted triangles* and *stippled line*) and to both solutions (*triangles* and *interrupted line*). The individual points represent averages for all well-defined transitions at the indicated potential.
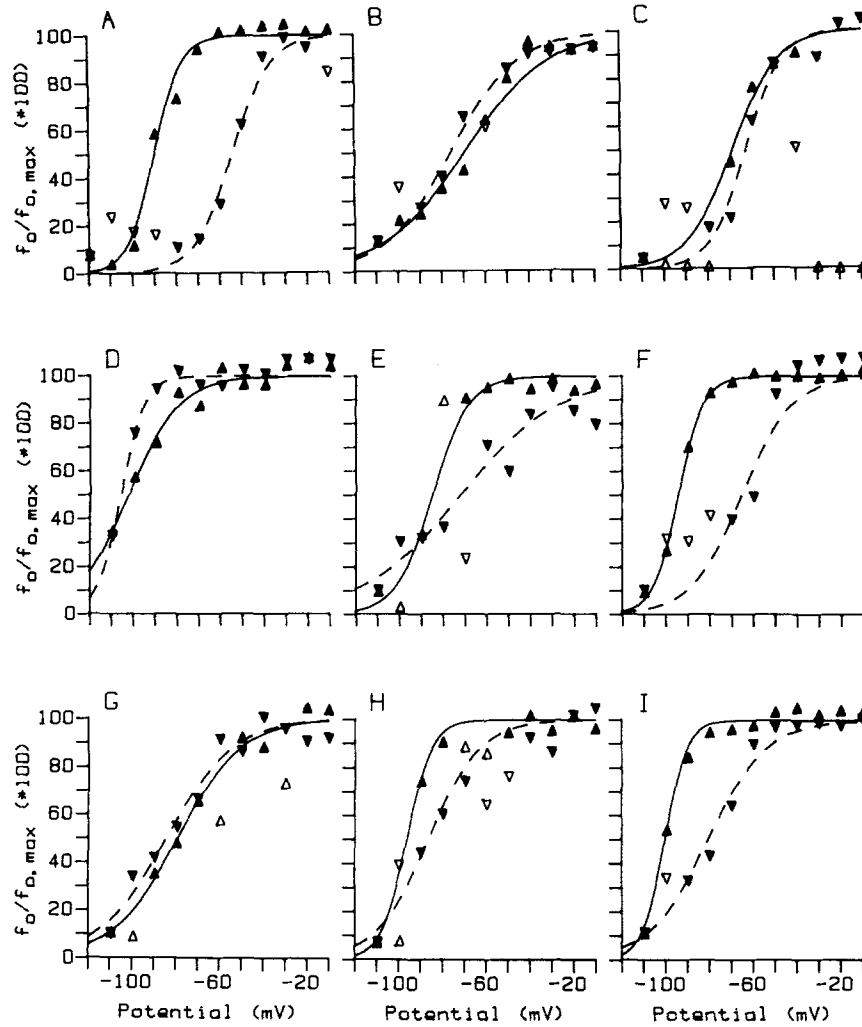
FIGURE 6. Intrachannel gating variability in a BTX-modified sodium channel in symmetrical 0.1 M NaCl plus 0.005 M $BaCl_2$ (protocol II). The nine panels depict the results of successive gating runs in a single channel. Exp. L50. For each gating run (panel), V_a and z_a are listed for the hyperpolarizing sequence first. (*A*) $V_a = -90$ mV, $z_a = 4.1$; $V_a = -54$ mV, $z_a = 2.9$. (*B*) $V_a = -69$ mV, $z_a = 1.4$; $V_a = -76$ mV, $z_a = 1.7$. (*C*) $V_a = -69$ mV, $z_a = 2.4$; $V_a = -62$ mV, $z_a = 3.1$. (*D*) $V_a = -102$ mV, $z_a = 2.2$; $V_a = -106$ mV, $z_a = 4.7$. (*E*) $V_a = -85$ mV, $z_a = 3.0$; $V_a = -72$ mV, $z_a = 1.1$. (*F*) $V_a = -94$ mV, $z_a = 4.4$; $V_a = -64$ mV, $z_a = 2.5$. (*G*) $V_a = -79$ mV, $z_a = 1.8$; $V_a = -84$ mV, $z_a = 1.7$. (*H*) $V_a = -97$ mV, $z_a = 4.8$; $V_a = -86$ mV, $z_a = 2.2$. (*I*) $V_a = -100$ mV, $z_a = 4.9$; $V_a = -81$ mV, $z_a = 1.9$. Symbols and curves as in Fig. 3.

TABLE III

Variability in Ba^{2+}-induced Gating Shifts

Expt	Control		With Ba^{2+}		Difference	
	V_a (hyp)	V_a (dep)	V_a (hyp)	V_a (dep)	Hyp	Dep
			mV			
			Symmetrical Ba^{2+}			
L21*	−116	−104	−109	−111	+7	−7
L23*	−119	−120	−110		+9	
L42	−110	−111	−94	−76	+16	+35
L45	−115	−117	−103	−107	+12	+10
L47	−106	−112	−106	−104	0	+9
L49	−108	−111	−104	−89	+4	+22
L50	−105	−113	−90	−54	+15	+59
			Asymmetrical Ba^{2+}			
L24	−100	−116	−94	−101	+6	+15
L27	−98	−92	−98	−70	0	+22
L34	−122	−126	−103		+19	
L35	−104	−107	−88		+16	
L40	−118	−119	−102	−106	+16	+13
L41	−125	−123	−102		+23	

Results obtained with protocol II. *Single-channel experiments, except for L21 (four channels) and L23 (two channels). Control: symmetrical 0.1 M NaCl. Symmetrical Ba^{2+}: symmetrical 0.1 M NaCl + 0.005 M $BaCl_2$. Asymmetrical Ba^{2+}: symmetrical 0.1 M NaCl + 0.005 M extracellular $BaCl_2$.

For each experiment, V_a is listed for the last hyperpolarizing and depolarizing control gating run and the first Ba^{2+} gating run. Where only information for the hyperpolarizing sequence is listed, the membrane broke before the depolarizing sequence was completed.
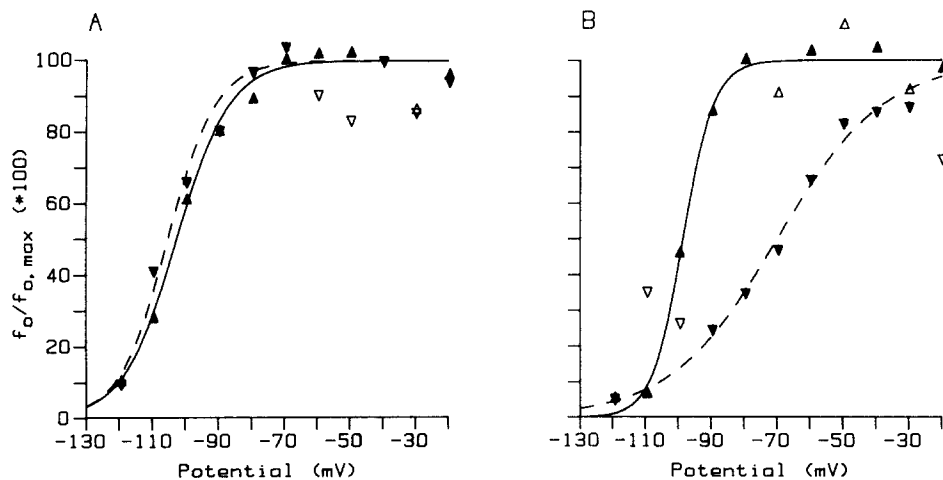

FIGURE 7. Single-channel gating curves in symmetrical 0.1 M NaCl after asymmetrical addition of 0.005 M $BaCl_2$ to the extracellular solution only (protocol II). (A) Exp. L40: V_a = −102 mV, z_a = 3.2 (hyperpolarizing); V_a = −106 mV, z_a = 3.5 (depolarizing). (B) Exp. L27: V_a = −98 mV, z_a = 5.4 (hyperpolarizing); V_a = −70 mV, z_a = 1.6 (depolarizing). Symbols and curves as in Fig. 3.

Divalent cations, however, produce voltage-dependent block of voltage-dependent sodium channels (Woodhull, 1973; Yamamoto et al., 1984; Worley et al., 1986; Nilius, 1988), and might also alter the single-channel conductance by screening fixed charges at the channel entrance (Green et al., 1987). Voltage-dependent changes in the time-averaged channel conductance may thus result from changes in the single-channel conductance as well as in channel activation. To evaluate the extent of this problem, ensemble-averaged single-channel i-V relations were constructed from well-resolved current transitions in the individual current traces (Fig. 5). In symmet-

TABLE IV

Effect of Ba^{2+} on Sodium Channel Gating

	Hyperpolarizing	Depolarizing	Combined	Range
	Asymmetrical Ba^{2+} addition			
V_a (mV)	-94 ± 11 (9)	-93 ± 16 (4)	-94 ± 12 (13)	$-69/-106$
z_a	3.3 ± 0.9	2.5 ± 0.8	3.1 ± 0.9	$1.6/5.4$
$g \cdot f_{o,max}$ (pS)	18.2 ± 2.5	18.8 ± 2.6	18.4 ± 2.5	$13.7/21.0$
G_b (pS)	5.0 ± 0.6	5.1 ± 0.1	5.0 ± 0.5	$3.6/5.9$
	Symmetrical Ba^{2+} addition			
V_a (mV)	-93 ± 14 (26)	-88 ± 17 (21)	-91 ± 16 (47)	$-54/-114$
z_a	3.4 ± 1.3	2.7 ± 1.1	3.1 ± 1.3	$1.1/6.2$
$g \cdot f_{o,max}$ (pS)	13.0 ± 1.7	13.2 ± 1.5	13.1 ± 1.6	$8.6/17.5$
G_b (pS)	7.2 ± 2.5	7.3 ± 1.9	7.3 ± 2.1	$3.2/11.7$
V_a^* (mV)	-91 ± 14 (23)	-87 ± 17 (20)	-89 ± 16 (43)	$-54/-114$
z_a^*	3.4 ± 0.9	2.7 ± 0.8	3.1 ± 1.3	$1.1/6.1$
$g \cdot f_{o,max}^*$	12.9 ± 1.8	13.2 ± 1.5	13.0 ± 1.7	$8.6/17.5$

Experiments in symmetrical 0.1 M NaCl plus symmetrical or asymmetrical 0.005 mM $BaCl_2$ (protocol II). Mean $\pm$ SD (number), obtained by averaging results from the individual gating sequences. V_a, z_a, and $g \cdot f_{o,max}$, denote estimates from the curve fits; G_b denotes the measured background conductance. Results in asymmetrical Ba^{2+} are based on six membranes each containing a single channel. Results in symmetrical Ba^{2+} are based on eight membranes with one to three channels (43 single-channel gating sequences). *Estimates based on the 43 single-channel gating sequences.

rical 0.1 M NaCl or 0.1 M NaCl plus 0.005 M $BaCl_2$, the i-V relations were approximately linear over most of the gating range. The small-signal conductances (g, determined at -20 mV $\leq V \leq 20$ mV) were 20.8 ± 0.5 (mean $\pm$ SD) and 12.6 ± 0.5 pS, respectively. In symmetrical 0.1 M NaCl, when 0.005 M $BaCl_2$ was added to only the extracellular solution, the i-V relation was nonlinear throughout the gating range, g was 17.8 ± 0.4 pS, and f_o was determined by "correcting" for the i-V nonlinearity (cf. Eq. 1).

Gating variability. In symmetrical 0.1 M NaCl, addition of 0.005 M $BaCl_2$ to both sides of the membrane produced a depolarizing shift in V_a, but there was a large

variability in the gating behavior. The intrachannel variability is illustrated in Fig. 6, which shows the hyperpolarizing and depolarizing sequences for nine consecutive gating runs on a single channel. (The interchannel variability is comparable to that illustrated in Fig. 6, results not shown.)

The interchannel variation in the response to symmetrical Ba^{2+} addition is illustrated in Table III, which summarizes information about the shift in V_a that is seen when comparing the last control gating run with the first Ba^{2+} gating run (for both symmetrical and asymmetrical Ba^{2+} addition). The individual shifts vary between -7 and $+59$ mV! The results in Table III also show that the shift was larger in the depolarizing sequences. Incomplete electrolyte mixing was ruled out by examination of the single-channel current records, which showed that the full Ba^{2+}-induced single-channel conductance decrease occurred before the start of the measurements.
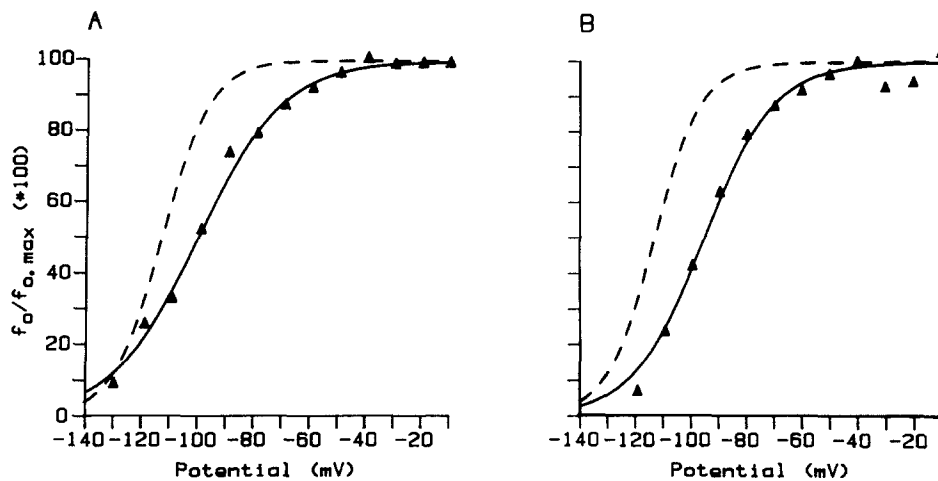

FIGURE 8.   Ensemble-averaged gating curves in symmetrical 0.1 M NaCl after addition of 0.005 M $BaCl_2$ to both electrolyte solutions, or to the extracellular solution only (protocol II). At each potential, the points denote the average $f_o/f_{o,max}$ based on all gating sequences obtained for that condition. The solid curves denote fits to the data. The interrupted curves denote the ensemble-averaged gating curve from Fig. 4. (A) After symmetrical addition: $V_a = -102$ mV, $z_a = 1.9$. (B) After asymmetrical addition: $V_a = -97$ mV, $z_a = 2.5$.

Addition of 0.005 M $BaCl_2$ to the extracellular solution only also produced a depolarizing shift in the gating curves. There was, again, considerable variability in gating behavior, as illustrated in Fig. 7. The interchannel variation in the response to extracellular Ba^{2+} addition is summarized in Table III.

Average gating behavior. Table IV summarizes the results of fitting all the individual gating experiments done in symmetrical 0.1 M NaCl plus symmetrical or asymmetrical 0.005 M $BaCl_2$. The results are summarized in terms of the three gating parameters (V_a, z_a, and $g·f_{o,max}$) for the hyperpolarizing and depolarizing sequences, separately as well as combined. There was, again, a large variability in the parameter estimates, with the largest variability among the depolarizing sequences. We do not understand the molecular basis for this increased variability.

Again, for each experimental condition (symmetrical or asymmetrical Ba^{2+}) we also

constructed an ensemble-averaged gating curve (based on all the individual gating curves obtained for each condition), where all the results obtained at each membrane potential were averaged together to construct f_o-V relations (Fig. 8 and Table V) for comparison with the ensemble-averaged f_o-V relation in 0.1 M NaCl. When fitting Eq. 3 to the ensemble-averaged f_o-V relation in asymmetrical Ba^{2+}, the estimate for V_a (-97 mV) did not differ significantly from that based on the average V_a of the fits to the individual gating runs (-94 ± 3 mV, mean $\pm$ SEM). The ensemble-averaged z_a (2.5) was less than the estimate obtained from averaging the estimates from the individual fits (3.1), but the difference was less than in symmetrical 0.1 M NaCl. When fitting Eq. 3 to the ensemble-averaged f_o-V relation in symmetrical Ba^{2+}, the ensemble-averaged V_a (-102 mV) differed by 11 mV from the average V_a (-91 ± 2 mV, mean $\pm$ SEM), and the ensemble-averaged z_a (1.9) was much less than the average z_a (3.1). The large difference between the latter two estimates for V_a results in part from the increased gating variability in symmetrical Ba^{2+} (Table IV), such that many more points were excluded from the fits to the individual curves (Figs. 6 and 7).

TABLE V

Summary of the Ensemble-averaged Gating Curves

Experimental condition	V_a	z_a
	mV	
0.1 M NaCl	-114	2.8
+0.005 M BaCl$_2$ (extracellular)	-97	2.5
+0.005 M BaCl$_2$ (symmetrical)	-102	1.9

Results obtained using protocol II. For each experimental condition, the time-averaged current for all gating sequences were averaged together; the average background conductance was calculated using the same weighting as for the individual sequences, and Eq. 3 was fitted to the results.

Based on the ensemble-averaged results (Fig. 8), symmetrical addition of (0.005 M) Ba^{2+} produced a 12-mV depolarizing shift in V_a, from -114 to -102 mV. Asymmetrical addition of Ba^{2+} to the extracellular solution only produced a 17-mV depolarizing shift in V_a, from -114 mV to -97 mV. By subtraction, Ba^{2+} when added to the intracellular solution shifts the gating curve 5 mV in the hyperpolarizing direction. Qualitatively, these shifts are consistent with those found when changing only the monovalent salt concentration (Table II), although the shift induced by intracellular Ba^{2+} is approximately threefold larger than would be predicted from the NaCl results (see Discussion).

DISCUSSION

In this article we have exploited two advantages of bilayer-incorporated, BTX-modified sodium channels: BTX appears to remove most types of inactivation (Khodorov, 1985); and one can with comparative ease "isolate" single functional channels in a bilayer. It is thus possible to examine the steady-state gating behavior of single voltage-dependent sodium channels. Furthermore, steady-state gating can to a first approximation be analyzed using a two-state model (Moczydlowski et al., 1984;

French et al., 1986; but see Keller et al., 1986 and Behrens et al., 1989). The increased resolution allowed by examining steady-state gating of single channels also reveals that there is a large intrachannel as well as interchannel variability in the gating behavior, which complicates the analysis of ionic strength–induced changes in channel gating.

We first discuss the gating variability. Next, we address the electrolyte-dependent modulation of sodium channel gating behavior and the associated question of channel asymmetry. We then estimate the intrinsic conformational free energy change involved in voltage activation. Finally, we address some implications for interpreting the results of pharmacological and other interventions in channel function.

Gating Variability: Multiplicity of Gating States

A striking feature of single BTX-modified sodium channels is the spontaneous changes in f_o at a constant V (Fig. 2). The changes in f_o were much larger than could be accounted for by statistical measuring errors, and were seen with most channels. They would presumably be observed with all channels if they were observed for a sufficiently long time, and may account for most (or all) of the interchannel gating variability.

Similar changes in f_o have been reported for other (bilayer-incorporated, BTX-modified) sodium channels: rat muscle (Moczydlowski et al., 1984); rat brain (French et al., 1986; Cukierman et al., 1988); electric eel (Recio-Pinto et al., 1987); squid optic nerve (Behrens et al., 1989); and human brain (Frenkel et al., 1990). Thus, the changes in f_o and the associated variability in gating behavior are not consequences of a particular set of experimental procedures, and the reported variability in V_a for other sodium channel types is similar to that found here: the standard deviation of V_a was ~15 mV for channels from either rat brain (Keller et al., 1986; Cukierman et al., 1988) or electric eel (Recio-Pinto et al., 1987; Shenkel et al., 1989), and ~10 mV for channels from human brain (Frenkel et al., 1990). The gating variability is not a sign of slow "rundown" or some other indicator of irreversible changes, because repeated gating runs in the same channel show reversible transitions between gating states with no consistent drift in gating behavior (Figs. 2, 3, 6, and 7), and similar estimates for V_a and z_a were obtained using two different protocols (Tables I and II). Specifically, the variations in gating behavior cannot be ascribed to the long depolarizations (at +60 mV) that were used in protocol II, because similar variations were observed in channels that were held at potentials close to V_a for prolonged periods of time (results not shown; see also O'Connell and Andersen, 1991).

The gating variability is thus an intrinsic channel property, in the sense that a given channel can exist in a number of different, interconverting states in which it has different gating behaviors. The molecular basis for the changes in gating behavior (e.g., the large changes in z_a seen in Figs. 3, C and D, 6, and 7 B) are obscure, however. Nor is it clear from these results whether the variability in gating behavior results because BTX-modified sodium channels possess a near continuum of gating states or because of transitions among a small number of discrete gating modes (cf. O'Connell and Andersen, 1991).

The question remains whether the variability in steady-state gating arises as a

consequence of the BTX modification or bilayer incorporation. That does not appear to be the case, because "native" sodium channels (in perfused giant axons, cell-detached patches, or cell-attached patches in muscle fiber segments, or expressed in *Xenopus* oocytes) also exhibit a multiplicity of gating states (Matteson and Armstrong, 1982; Horn et al., 1984; Patlak and Ortiz, 1985, 1989; Nilius, 1988; Moorman et al., 1990). (In single-channel experiments, the existence of multiple gating states is discernible as the nonrandom clustering of traces with similar gating behavior [cf. Nilius, 1988], with spontaneous transitions among the different gating behaviors.) It remains an open question, however, whether sodium channels in intact cells exhibit similar gating variations.

Depending on how long a channel stays in a given gating state, the variation in single-channel gating can show up as simple, parallel, or nonparallel shifts in the steady-state gating curves, or as seemingly uncontrolled variability (Figs. 2, 3, 6, and 7). The simple (parallel) shifts are similar to those induced by changes in the aqueous electrolyte composition, and complicate considerably the analysis of such changes because of the need to distinguish between spontaneous and induced gating changes. This is a particular problem because channels can remain in a given gating state for many minutes, and thus may appear to have a stable gating pattern.

Because of the gating variability, z_a is larger when estimated from single-channel gating runs than when estimated from the ensemble-averaged data (Tables I, IV, and V): based on analysis of the single-channel gating runs in symmetrical 0.1 M NaCl (protocol II), z_a was 3.7 ± 0.1 (mean ± SEM), but was only ~2.8 for the ensemble-averaged results obtained by averaging the results from all experiments obtained using protocol II (cf. Fig. 4). Similarly, based on analysis of the individual gating runs in symmetrical 0.1 M NaCl + 0.005 M BaCl, z_a was 3.1 ± 0.2 (mean ± SEM), but was only ~1.9 for the ensemble-averaged results (cf. Fig. 8 *A*). The ensemble-averaged results correspond to what would be observed in conventional, macroscopic voltage-clamp experiments (on BTX-modified sodium channels). Care should thus be exerted when assigning mechanistic or molecular significance to estimates of z_a based on macroscopic voltage-clamp experiments.

Estimates for V_a were relatively less affected by whether they were obtained by averaging the individual estimates or from analysis of the ensemble-averaged results (Table V). V_a's for the ensemble-averaged curves were "shifted" in the hyperpolarizing direction, but the difference was only significant for the experiments in symmetrical 0.1 M NaCl + 0.005 M BaCl, where there was a 11-mV difference between the two estimates. Since many points were excluded from the analysis of the individual experiments (cf. Fig. 6), we consider the ensemble-averaged estimate to be the more representative. Consequently, these estimates will be used to analyze the Ba^{2+} results further (see below).

Channel Asymmetry and Electrolyte-dependent Gating Shifts

Based on results on sodium channel gating obtained with the squid giant axon (Chandler et al., 1965) and frog myelinated nerve (Hille et al., 1975), the extracellular and intracellular channel (or membrane) surfaces appear to differ in apparent charge density. (In fact, the charge distribution at either surface is likely to be inhomogeneous, as Smith-Maxwell and Begenisich [1987] found that the apparent

charge density in the vicinity of the intracellular channel entrance in the squid giant axon differed approximately fourfold from the charge density deduced from gating experiments.) With respect to channel gating, the apparent charge density at the extracellular surface was estimated to be three to five times larger than that of the intracellular surface (Hille et al., 1975). Presumably, this asymmetry reflects a real difference between the extracellular and the intracellular channel surfaces in the vicinity of the channel's voltage sensor(s), because the average charge density at the intracellular membrane surface of the node of Ranvier is higher than that at the extracellular membrane surface (Benz and Nonner, 1981; Cahalan and Hall, 1982). But the question of species differences and the existence of multiple neuronal isochannels (e.g., Numa, 1989) that are differentially regulated (Gordon et al., 1987; Beckh et al., 1989; Beckh, 1990) raise uncertainties about the deduced asymmetry in charge density.

Clear-cut evidence for channel asymmetry was provided by Cukierman et al. (1988), who showed that symmetrical addition of 0.0075 M $CaCl_2$ to channels bathed in 0.15 M NaCl produced a 10-mV depolarizing shift in the gating curve, irrespective of whether the host bilayer was neutral or carried a net negative charge. It is unclear, however, how the shift should be partitioned into contributions from differential Ca^{2+} binding and screening of fixed charges. Hille et al. (1975) found that when 0.001–0.01 M divalent cations were added to the extracellular solution of a node of Ranvier, Ca^{2+} induced an ~ 5 mV larger shift than Ba^{2+}, which is evidence for Ca^{2+} binding.

In this article we confirm and extend the results of Cukierman et al. (1988): symmetrical increases in the concentration of monovalent salt (NaCl) and symmetrical additions of $BaCl_2$ both induce depolarizing shifts in the steady-state gating curves of BTX-modified sodium channels. The [NaCl]-induced changes in V_a occur without significant changes in z_a, which suggests that the shifts in V_a result simply from differential changes in V_s at the two channel surfaces. Addition of Ba^{2+}, however, either to the extracellular or to the intracellular solution, decreases z_a, which suggests that Ba^{2+}, in addition to its screening action, also interacts specifically with the channel. For that reason, the [NaCl]-induced shifts in V_a were used to estimate the apparent extracellular and intracellular surface charge densities, which then were used to predict the [Ba^{2+}]-induced shifts as a consistency test.

For the analysis, the [NaCl]-induced shifts in the gating curve were assumed to arise from changes in uniform surface potentials that result from simple screening of fixed surface charges as described by the Gouy-Chapman theory of the diffuse double layer (e.g., Aveyard and Haydon, 1973; McLaughlin, 1977). In this approximation, the surface charge density (σ), surface potential (V_s), and electrolyte composition are related by:

$$\sigma = (A/2)\cdot\left\{\sum_i [I]_i\cdot[\exp\{-z_i\cdot V_s\cdot e/(k\cdot T)\} - 1]\right\}^{0.5} \tag{4}$$

where A is a constant (= $[8\cdot k\cdot T\cdot\epsilon_o\cdot\epsilon_r]^{0.5}$, ϵ_o is the permittivity of free space, and ϵ_r is the relative dielectric constant), while $[I]_i$ and z_i denote the concentration and valence of ion species i.

For a uni-univalent electrolyte, Eq. 4 is solved exactly for V_s as a function of σ and

the salt concentration (C):

$$V_s = (2 \cdot k \cdot T/e) \cdot \sinh^{-1}\{\sigma/(A \cdot C^{0.5})\} \tag{5a}$$

$$= (2 \cdot k \cdot T/e) \cdot \ln\{\sigma/(A \cdot C^{0.5}) + [\sigma^2/(A^2 \cdot C) + 1]^{0.5}\} \tag{5b}$$

A change in the aqueous electrolyte concentration, from C_1 to C_2, produces the following change in surface potential:

$$V_{s,2} - V_{s,1} = (2 \cdot k \cdot T/e) \cdot \ln \left[\frac{\sigma/(A \cdot C_2^{0.5}) + [\sigma^2/(A^2 \cdot C_2) + 1]^{0.5}}{\sigma/(A \cdot C_1^{0.5}) + [\sigma^2/(A^2 \cdot C_1) + 1]^{0.5}} \right] \tag{6}$$

Eq. 6 was solved numerically (by Newton-Raphson iteration) to obtain estimates for σ given the measured shifts in V_s.

The extracellular and intracellular apparent surface charge densities (σ_e and σ_i) were estimated by assuming that the shifts in V_a result solely from changes in the extracellular and the intracellular surface potentials (V_s^e and V_s^i):

$$V_a = V_a + V_s^e - V_s^i \tag{7}$$

where V_a denotes the intrinsic ([NaCl]-independent) midpoint potential, which would be observed if there were no surface potentials.

First, σ_i was estimated from the 19-mV hyperpolarizing shift in V_a that was produced by changing the intracellular [NaCl] from 0.02 to 0.1 M. A hyperpolarizing shift in V_a corresponds to a positive change in V_s^i(cf. Eq. 7), and σ_i was estimated to be about -0.08 $e \cdot nm^{-2}$ (with an uncertainty of ~ 0.03 $e \cdot nm^{-2}$, as estimated by imposing ± 5-mV changes on the shift in V_a).

Next, σ_e was estimated by converting the measured shifts in V_a to changes in V_s^e after correcting for the [NaCl]-dependent changes in V_s^i. When [NaCl] was increased symmetrically, from 0.1 to 0.5 M, V_a shifted by $+20$ mV, but V_s^i was predicted to change by $+10$ mV, such that the actual change in V_s^e was approximately $+30$ mV, and σ_e was estimated to be -0.37 $e \cdot nm^{-2}$. Using the 0.1–1.0 M results, the corresponding numbers were as follows: the shift in V_a was 34 mV, the change in V_s^e was predicted to be $+12$ mV, the predicted change in V_s^e was thus approximately $+46$ mV, and σ_e was estimated to be -0.54 $e \cdot nm^{-2}$. Using the 0.5–1.0 M results, σ_e was finally estimated to be -1.3 $e \cdot nm^{-2}$. The variation in the σ_e estimates as a function of [NaCl] may result because the local [H$^+$], and thus the protonation of channel-associated charges, varies with V_s (Hille et al., 1975). But the σ_e variation could also arise because of the problems in using the Gouy-Chapman theory (see below) or because of experimental uncertainty. Thus, in the following we use the average of the above estimates, about -0.7 $e \cdot nm^{-2}$.

The use of the Gouy-Chapman theory is an oversimplification: the surfaces of a sodium channel are of finite area and they are nonplanar (Demin et al., 1986); and the charges will be relatively fixed, probably not uniformly distributed over the channel surfaces, and certainly not uniformly smeared. The electrostatic potential at the channel surface will thus show local nonuniformities, and the estimated charge densities will be apparent charge densities. They should be regarded as phenomenological descriptors of the results, to be used for comparison with other data (e.g., Tables I and II in Gilbert and Ehrenstein, 1984).

In that context, the apparent charge densities, $\sigma_e \approx -0.7\ e\cdot nm^{-2}$ and $\sigma_i \approx -0.08$ $e\cdot nm^{-2}$, are in general agreement with the estimates obtained by other workers on a variety of native sodium channels: $\sigma_e \approx -1.0\ e\cdot nm^{-2}$ and $\sigma_i \approx -0.14\ e\cdot nm^{-2}$ (e.g., Gilbert and Ehrenstein, 1984). The charge density estimates for channels in their native environment are numerically larger than ours, possibly because we examined channels in neutral membranes while the estimates for native channels contain an additional contribution from negative charges in the host membrane. Cukierman et al. (1988) thus found that the Ca^{2+}-induced shifts were ~ 7 mV larger in magnitude for channels in net negative membranes than for channels in neutral membranes.

Our experiments were done with sodium channels in neutral bilayers, and the lipids that surround the channels in the native membrane should have been replaced by the phospholipids of the planar bilayer. Integral membrane proteins exhibit only modest lipid specificity (Devaux and Seigneuret, 1985), and lipids that were introduced into the bilayer with the channel should be exchanged by the lipids in the host bilayer. The deduced surface charges should thus be integral to the sodium channel itself (cf. Cukierman et al., 1988). The general agreement between the different apparent surface charge estimates (see above) suggests that the underlying charges are a conserved feature of voltage-dependent sodium channels.

Divalent cations may alter channel gating by screening fixed surface charges, by specific binding to the surface (which will alter the net charge density), or by a combination of these effects (McLaughlin, 1977). In addition, divalent cations may alter gating if they bind and thereby alter the standard free energy for channel activation, which would alter gating by mechanisms that are not related to changing the field in the voltage-sensing regions. Ion binding could also alter the distribution among different gating states, which would become evident as a change in the ensemble-averaged z_a.

If Ba^{2+} addition shifted the gating curves solely by screening the fixed surface charges, the Ba^{2+}-induced shifts should be predicted from the results obtained when changing only [NaCl] using Eq. 4. For $\sigma_e = -0.7\ e\cdot nm^{-2}$, addition of 0.005 M $BaCl_2$ to an extracellular solution containing 0.1 M NaCl is predicted to produce a 17-mV depolarizing shift in V_a. Given the uncertainties inherent in using the Gouy-Chapman theory, this is in surprisingly good agreement with the observed shift of 17 mV (Table V). For $\sigma_i = -0.08\ e\cdot nm^{-2}$, addition of 0.005 M $BaCl_2$ to an intracellular solution containing 0.1 M NaCl is predicted to produce a 1.4-mV hyperpolarizing shift in V_a. The observed shift is threefold larger, 5 mV (Table V). Given the experimental uncertainty and the limitations involved in using the Gouy-Chapman theory to predict the shift, one should probably not ascribe mechanistic significance to the discrepancy per se.

Specific Ba^{2+} interactions. Nevertheless, Ba^{2+} interacts specifically with voltage-dependent sodium channels because Ba^{2+} addition decreases z_a for the ensemble-averaged gating curves (Tables I and V), with the largest effect after symmetrical Ba^{2+} addition (see also Cukierman and Krueger, 1990). The decreased z_a results from an increased variability among the individual gating curves (Table V). There is also a decrease in z_a for the individual curves, with the largest decrease for the depolarizing gating runs, which could reflect a "true" Ba^{2+}-induced alteration in z_a, or an increased variability within the individual gating runs. The Ba^{2+}-induced increase in gating variability probably results from specific binding to the intracellular channel surface,

but it could also arise because of alterations in the local potential along the channel surface (i.e., because of nonuniform screening). We do not favor the latter possibility, however, because the [NaCl]-induced shifts were larger than the [Ba^{2+}]-induced shifts and not associated with changes in z_a.

Ba^{2+} addition also alters Na^+ permeation through the channel (and may itself be slightly permeant [cf. Khodorov and Revenko, 1979]). When Ba^{2+} was added to the extracellular solution only (0.005 M $BaCl_2$ to 0.1 M NaCl), the i-V relation was nonlinear (Fig. 5). In the gating voltage range (−40 to −110 mV), the single-channel chord conductance varied between 90 and 60% of the small-signal conductance (17.8 ± 0.4 pS). When Ba^{2+} was added symmetrically (0.005 M $BaCl_2$ to 0.1 M NaCl), the i-V relation was approximately linear (to −100 mV) and the small-signal conductance was 12.6 ± 0.8 pS, which should be compared with the conductance in 0.1 M NaCl alone, 20.8 ± 0.5 pS. Ba^{2+} addition will alter the electrostatic potential at the channel entrance, which alters the local [Na^+] at the entrances and thus the single-channel conductance (Green et al., 1987; Cai and Jordan, 1990):

$$g = g_{max} \cdot [Na^+]_b / \{[Na^+]_b + K_{Na} \cdot exp(-V_e \cdot z/kT)\} \tag{8}$$

where g_{max} and K_{Na} denote the maximal single-channel conductance and Na^+ dissociation constant, respectively, [Na^+]$_b$ is the bulk Na^+ concentration, and V_e is the electrostatic potential at the channel entrances (which are assumed to have symmetrical charge densities). The Ba^{2+}-induced changes in V_e were estimated from Eqs. 4 and 8, assuming an apparent charge density at the entrances of $-0.38 \, e \cdot nm^{-2}$, $g_{max} = 45$ pS, and $K_{Na} = 1.5$ M (Green et al., 1987). g is thus predicted to decrease, from 20.6 pS in symmetrical 0.1 M NaCl to 16.7 pS in 0.1 M NaCl + 0.005 M $BaCl_2$. We can account for ~50% of the Ba^{2+}-induced conductance decrease. That we predict a too-little conductance decrease may be because the model is too crude (cf. Cai and Jordan, 1990), or because Ba^{2+} binds to the channel to either block the pore or alter V_e more than predicted.

The rather modest i-V nonlinearity in asymmetrical Ba^{2+} nevertheless affects the steady-state (time-averaged) single-channel currents, because not only f_o but also $g(V)$ varies as a function of V. If the gating curves were analyzed without correction for the i-V nonlinearity, V_a for the ensemble-averaged gating curve would be −93 mV, or 4 mV positive to the "true" estimate, in which case the Ba^{2+}-induced shift would appear to be 21 mV and one might conclude that Ba^{2+} interacts specifically with the extracellular channel surface.

Other divalent cations (e.g., Ca^{2+} and Zn^{2+}) produce more pronounced nonlinearities in the single-channel i-V relations (Yamamoto et al., 1984; Weiss and Horn, 1986; Worley et al., 1986; Green et al., 1987), which appear to result from a Woodhull-type voltage-dependent block of the open channels (Woodhull, 1973), and it becomes correspondingly more important to correct for the effect of these ions on the single-channel i-V.

The Standard Free Energy of Channel Activation

In the two-state approximation, the standard free energy for the conformational changes underlying channel activation ΔG_a^o (at $V = 0$ mV) is given by:

$$\Delta G_a^o = z_a \cdot e \cdot V_a \tag{9}$$

where V_a is the midpoint potential that would be observed when $V_s^e = V_s^i = 0$. The measured V_a contains contributions from V_a, as well as the two surface potentials, V_s^e and V_s^i (see Eq. 7). V_a can thus be estimated from the measured V_a and the estimated surface potentials. In 0.1 M NaCl, $V_a \approx -110$ mV; using Eq. 4 and our estimates for σ_e and σ_i, V_s^e and V_s^i are predicted to be -94 and -17 mV, respectively. V_a is thus about -30 mV, z_a is ~ 3.7 (Table I), and $\Delta G_a^o \approx -12$ kJ/mol. This corresponds to the formation of a hydrogen bond (Schulz and Schirmer, 1979, Table 3.1), or the removal of a single monovalent charge of radius 0.2 nm from a uniform medium of dielectric constant 30 (as calculated from the Born equation [e.g., Bockris and Reddy, 1970]).

ΔG_a^o may be underestimated in magnitude because z_a may be underestimated. If, for example, the channels undergo rapid transitions between two (or more) gating states, which are not discernible in the heavily filtered (50 Hz) current traces we use to determine f_o, the f_o-V relation will be less steep than if the channels remained in a single gating state. Nevertheless, the energetic cost of activating (BTX-modified) sodium channels is modest. (In native membranes, the gating curve for BTX-modified sodium channels is shifted ~ 40 mV in the hyperpolarizing direction as compared with unmodified channels [Khodorov and Revenko, 1979; Huang et al., 1982], which implies that ΔG_a^o for the unmodified channels is close to zero.)

Implications for Pharmacological and Other Studies

At first sight, the variability in the steady-state gating behavior of bilayer-incorporated, BTX-modified sodium channels appears larger than for native channels. But this is probably a consequence of the increased resolution of the steady-state measurements. Qualitatively, the gating machinery of native channels exhibits a variability (Horn et al., 1984; Nilius, 1988) that is consistent with the changes in V_a observed here. This raises the question of how one should interpret a shift in V_a, or a change in z_a, that results from some experimental intervention. The observed changes could occur as the direct result of the intervention (e.g., a change in the surface potential), or they could occur as the indirect consequence of altering the distribution among different gating states, or as the combination of both actions.

Specifically, symmetrical Ba^{2+} addition induces an increased variability in channel gating (Table IV), as reflected in the larger range of V_a for the individual single-channel gating curves and the decrease in z_a for the ensemble-averaged gating curve by 0.8 relative to the control curve (Fig. 8, Table V). The decrease in z_a could be interpreted to mean that Ba^{2+} addition alters the gating-related charge redistribution within the channel. But that is probably not the case: the primary cause for the decrease in z_a seems to be the increase in gating variability, which arises because Ba^{2+} binds at the intracellular channel surface.

We finally note that the ensemble-averaged gating curves (Figs. 4 and 8) are well fit by two-state Boltzmann distributions, even though the fitted curves have no obvious molecular significance. Even apparently "regular" macroscopic behavior does not ensure against the existence of an underlying molecular variability (on the second to minute timescale).

REFERENCES

Andersen, O. S., and R. U. Muller. 1982. Monazomycin-induced single channels. I. Characteristics of the elementary conductance events. *Journal of General Physiology.* 80:403–426.

Århem, P. 1980. Effects of some heavy metal ions on the ionic currents of myelinated fibres from *Xenopus laevis. Journal of Physiology.* 306:219–231.

Armstrong, C. M. 1981. Sodium channels and gating currents. *Physiological Reviews.* 61:644–683.

Aveyard, R., and D. A. Haydon. 1973. An Introduction to the Principles of Surface Chemistry. Cambridge University Press, London. 31–57.

Beckh, S. 1990. Differential expression of sodium channel mRNAs in rat peripheral nervous system and innervated tissues. *FEBS Letters.* 262:317–322.

Beckh, S., M. Noda, H. Lübbert, and S. Numa. 1989. Differential regulation of three sodium channel messenger RNAs in the rat central nervous system during development. *EMBO Journal.* 8:3611–3616.

Begenisich, T. 1975. Magnitude and location of surface charges on *Myxicola* giant axons. *Journal of General Physiology.* 66:47–65.

Begenisich, T., and C. Lynch. 1973. Effects of internal divalent cations on voltage-clamped squid axons. *Journal of General Physiology.* 63:675–689.

Behrens, M. I., A. Oberhauser, F. Bezanilla, and R. Latorre. 1989. Batrachotoxin-modified sodium channels from squid optic nerve in planar bilayers. Ion conduction and gating properties. *Journal of General Physiology.* 93:23–41.

Benz, R., and W. Nonner. 1981. Structure of the axolemma of frog myelinated nerve: relaxation experiments with a lipophilic probe ion. *Journal of Membrane Biology.* 59:127–134.

Bevington, P. R. 1969. Data Reduction and Error Analysis for the Physical Sciences. McGraw-Hill, New York. 204–246.

Bockris, J. O'M., and A. K. N. Reddy. 1970. Modern Electrochemistry. Vol. I. Publishing Corp. Plenum, New York. 45–72.

Brismar, T. 1973. Effects of ionic concentrations on permeability properties of nodal membrane in myelinated nerve fibres of *Xenopus laevis. Acta Physiologica Scandinavica.* 87:474–484.

Cahalan, M. D., and J. Hall. 1982. Alamethicin channels incorporated into frog node of Ranvier. Calcium-induced inactivation and membrane surface charges. *Journal of General Physiology.* 79:411–436.

Cai, M., and P. Jordan. 1990. How does vestibule surface charge affect ion conduction and toxin binding in a Na channel. *Biophysical Journal.* 57:883–891.

Chabala, L. D., B. W. Urban, L. B. Weiss, W. N. Green, and O. S. Andersen. 1989. Steady-state activation properties of batrachotoxin-modified sodium channels in lipid bilayers. *Society for Neuroscience Abstracts.* 15:537a. (Abstr.)

Chandler, W. K., A. L. Hodgkin, and H. Meves. 1965. The effect of changing the internal solution on sodium inactivation and related phenomena in giant axons. *Journal of Physiology.* 180:821–836.

Cohen, R. S., F. Blomberg, K. Berzins, and P. Siekevitz. 1977. The structure of postsynaptic densities isolated from dog cerebral cortex. *Journal of Cell Biology.* 74:181–203.

Cukierman, S., and B. K. Krueger. 1990. Modulation of sodium channel gating by external divalent cations: differential effects on opening and closing rates. *Pflügers Archiv.* 416:360–367.

Cukierman, S., W. C. Zinkand, R. J. French, and B. K. Krueger. 1988. Effects of membrane surface charge and calcium on the gating of rat brain sodium channels in planar bilayers. *Journal of General Physiology.* 92:431–447.

Demin, V. V., E. V. Grishkin, V. A. Kovalenko, and S. N. Spadar. 1986. Electron microscopy studies of the fast sodium channel structure. *In* Chemistry of Peptides and Proteins. Vol. 3. W. Voelter, E. Bayer, Y. A. Ovchinnikov, and V. T. Ivanov, editors. W. de Gruyter and Co., Berlin. 363–370.

Devaux, P. F., and M. Seigneuret. 1985. Specificity of lipid-protein interactions as determined by spectroscopic techniques. *Biochimica et Biophysica Acta.* 822:63–125.

Ehrenstein, G., H. Lecar, and R. Nossal. 1970. The nature of the negative resistance in bimolecular lipid membranes containing excitability-inducing material. *Journal of General Physiology.* 55:119–133.

Frankenhaeuser, B., and A. L. Hodgkin. 1957. The action of calcium on the electrical properties of squid axons. *Journal of Physiology.* 137:218–244.

French, R. J., J. F. Worley III, M. B. Blaustein, W. O. Romine, K. K. Tam, and B. K. Krueger. 1986. Gating of batrachotoxin-activated sodium channels in lipid bilayer membranes. *In* Reconstitution of Ion Channel Proteins. C. Miller, editor. Plenum Publishing Corp., New York. 363–383.

Frenkel, C., D. S. Duch, and B. W. Urban. 1990. Molecular actions of pentobarbital isomers on sodium channels from human brain cortex. *Anesthesiology.* 72:640–649.

Gilbert, D. L., and G. Ehrenstein. 1984. Membrane surface charge. *Current Topics in Membranes and Transport.* 22:407–421.

Gordon, D., D. Merrick, V. Auld, R. Dunn, A. L. Goldin, N. Davidson, and W. A. Catterall. 1987. Tissue-specific expression of the R_I and R_{II} sodium channel subtypes. *Proceedings of the National Academy of Sciences, USA.* 84:8682–8686.

Gottlieb, M. H. 1974. Binding of alkaline and alkaline earth cations in lecithin mesophases. *Journal of Colloid and Interface Science.* 48:394–399.

Green, W. N., L. B. Weiss, and O. S. Andersen. 1984. Batrachotoxin-modified sodium channels in lipid bilayers. *Annals of the New York Academy of Sciences.* 435:548–550.

Green, W. N., L. B. Weiss, and O. S. Andersen. 1987. Batrachotoxin-modified sodium channels in planar lipid bilayers: ion permeation and block. *Journal of General Physiology.* 89:841–872.

Grissmer, S. 1984. Effect of various cations and anions on the action of tetrodotoxin and saxitoxin on frog myelinated nerve fibers. *Pflügers Archiv.* 402:353–359.

Hartshorne, R. P., B. U. Keller, J. A. Talvenheimo, W. A. Catterall, and M. Montal. 1985. Functional reconstitution of the purified brain sodium channel in planar lipid bilayers. *Proceedings of the National Academy of Sciences, USA.* 82:240–244.

Henderson, P. 1907. Zur Thermodynamik der Flüssigkeitsketten. *Zeitschrift für Physikalische Chemie.* 59:118–127.

Hille, B. 1968. Charges and potentials at the nerve surface. Divalent ions and pH. *Journal of General Physiology.* 51:221–236.

Hille, B., A. M. Woodhull, and B. I. Shapiro. 1975. Negative surface charge near sodium channels of nerve: divalent ions, monovalent ions, and pH. *Philosophical Transactions of the Royal Society, B.* 270:301–318.

Horn, R., C. A. Vandenberg, and K. Lange. 1984. Statistical analysis of single sodium channels. Effects of N-bromoacetamide. *Biophysical Journal.* 45:323–335.

Huang, L.-Y. M., N. Moran, and G. Ehrenstein. 1982. Batrachotoxin modifies the gating kinetics of sodium channels in internally perfused neuroblastoma cells. *Proceedings of the National Academy of Sciences, USA.* 79:2082–2085.

Keller, B. U., R. P. Hartshorne, J. A. Talvenheimo, W. A. Catterall, and M. Montal. 1986. Sodium channels in planar lipid bilayers. Channel gating kinetics of purified sodium channels modified by batrachotoxin. *Journal of General Physiology.* 88:1–23.

Khodorov, B. I. 1985. Batrachotoxin as a tool to study voltage-sensitive sodium channels of excitable membranes. *Progress in Biophysics and Molecular Biology.* 45:57–148.

Khodorov, B. I., and S. V. Revenko. 1979. Further analysis of the mechanisms of action of batrachotoxin on the membrane of myelinated nerve. *Neuroscience.* 4:1315–1340.

Krueger, B. K., J. F. Worley III, and R. J. French. 1983. Single sodium channels from rat brain incorporated into planar lipid bilayer membranes. *Nature.* 303:172–175.

Matteson, D. R., and C. M. Armstrong. 1982. Evidence for a populations of sleepy sodium channels in squid axon at low temperature. *Journal of General Physiology.* 79:739–758.

McLaughlin, S. 1977. Electrostatic potentials at membrane-solution interfaces. *Current Topics in Membranes and Transport.* 9:71–144.

McLaughlin, S. G. A., G. Szabo, and G. Eisenman. 1971. Divalent ions and the surface potential of charged phospholipid membranes. *Journal of General Physiology.* 58:667–687.

Moczydlowski, E., S. S. Garber, and C. Miller. 1984. Batrachotoxin-activated Na^+ sodium channels in planar lipid bilayers: competition of tetrodotoxin block by Na^+. *Journal of General Physiology.* 84:665–686.

Moorman, J. R., G. E. Kirsch, A. M. J. VanDongen, R. H. Joho, and A. M. Brown. 1990. Fast and slow gating of sodium channels encoded by a single mRNA. *Neuron.* 4:243–252.

Mueller, P., and D. O. Rudin. 1963. Induced excitability in reconstituted cell membrane structure. *Journal of Theoretical Biology.* 4:268–280.

Nilius, B. 1988. Modal gating behavior of cardiac sodium channels in cell-free membrane patches. *Biophysical Journal.* 53:857–862.

Numa, S. 1989. A molecular view of neurotransmitter receptors and ionic channels. *The Harvey Lectures.* 83:121–165.

O'Connell, A. M., and O. S. Andersen. 1991. Identification and characterization of three distinct activation modes in BTX-modified sodium channels. *Biophysical Journal.* 59:260a. (Abstr.)

Patlak, J., and M. Ortiz. 1985. Slow currents through single sodium channels of the rat adult heart. *Journal of General Physiology.* 86:89–104.

Patlak, J. B., and M. Ortiz. 1989. Kinetic Diversity of Na^+ channel bursts in frog skeletal muscle. *Journal of General Physiology.* 94:279–301.

Recio-Pinto, E., D. S. Duch, S. R. Levinson, and B. W. Urban. 1987. Purified and unpurified sodium channels from eel electroplax in planar lipid bilayers. *Journal of General Physiology.* 90:375–395.

Robinson, R. A., and R. H. Stokes. 1965. Electrolyte Solutions. 2nd Ed. Rev. Butterworths, London. 571.

Schulz, G. E., and R. H. Schirmer. 1979. Principles of Protein Structure. Springer-Verlag, Berlin. 314.

Shenkel, S., E. C. Cooper, A. S. James, W. Agnew, and F. J. Sigworth. 1989. Purified, modified eel sodium channels are activated in planar bilayers in the absence of activating neurotoxins. *Proceedings of the National Academy of Sciences, USA.* 86:9592–9596.

Smith-Maxwell, C., and T. Begenisich. 1987. Guanidinium analogues as probes of the squid axon sodium pore. Evidence for internal surface charges. *Journal of General Physiology.* 90:361–374.

Steinhardt, J., and S. Beychok. 1964. Interaction of proteins with hydrogen ions and other small ions and molecules. *In* The Proteins: Composition, Structure and Function. 2nd ed. Academic Press, New York. 1:140–304.

Weiss, L. B., W. N. Green, and O. S. Andersen. 1984. Single-channel studies on the gating of batrachotoxin (BTX)-modified sodium channels in lipid bilayers. *Biophysical Journal.* 45:67a. (Abstr.)

Weiss, R. E., and R. Horn. 1986. Single-channel studies of TTX-sensitive and TTX-resistant sodium channels in developing rat muscle reveal different open channel properties. *Annals of the New York Academy of Sciences.* 479:152–161.

Woodhull, A. M. 1973. Ionic blockage of sodium channel in nerve. *Journal of General Physiology.* 61:687–708.

Worley, J. F., III, R. J. French, and B. K. Krueger. 1986. Trimethyloxonium modification of single batrachotoxin-activated sodium channels in planar bilayers. Changes in unit conductance and in block by saxitoxin and calcium. *Journal of General Physiology.* 87:327–349.

Yamamoto, D., J. Z. Yeh, and T. Narahashi. 1984. Voltage-dependent calcium block of normal and tetramethrin-modified single sodium channels. *Biophysical Journal.* 45:337–344.